Real-Time Attitude-Independent Gyro Calibration from Three-Axis Magnetometer Measurements

Kok-Lam Lai* and John L. Crassidis†

University at Buffalo, State University of New York, Amherst, NY 14260-4400

Richard R. Harman‡

NASA Goddard Space Flight Center, Greenbelt, MD 20771

A new real-time approach for gyro bias calibration using three-axis magnetometer measurements without any attitude knowledge is derived. This approach relies on a conversion of the three-axis magnetometer measurement and its derivative into an attitude-independent formulation. The goal is to use a calibrated three-axis magnetometer to determine the gyro biases before attitude information is available, which is often the case during orbit injection. Real-time algorithms are derived based on the Unscented filter, which is more robust to initial errors than an extended Kalman filter. The new formulation is tested with realistically simulated data based on the Tropical Rainfall Measurement Mission spacecraft. Simulation results indicate that accurate gyro bias calibration is possible.

I. Introduction

THREE-axis magnetometers (TAMs) are widely used for onboard spacecraft operations. The basic concept behind these devices is a fairly simple one, involving a magnetic sensor coupled with an electronics unit to provide data in a digital format. These sensors are useful since they provide both the direction and magnitude of the magnetic field; they are lightweight, reliable, and have low power requirements, with no moving parts.[1] For these reasons most low-Earth orbiting spacecraft (below 1000 km) have TAMs as part of their basic sensor package. It is well known that a TAM can be used to determine a three-axis attitude when coupled with gyros or a dynamic model in an extended Kalman filter.[2] Attitude-knowledge accuracies of 1-2 degrees are common using this approach, which can be improved by using well-calibrated sensors to achieve accuracies of 0.1-0.5 degrees.[3] An exciting new area of research involves using a TAM together with rate and sun sensor measurements for orbit (position) estimation. Accuracies on the order of 10 to 100 km can be achieved, which is within the position-knowledge requirements of many spacecraft.[4,5] These studies clearly show that an integrated magnetometer-based attitude/orbit estimation system can provide the necessary knowledge requirements of a spacecraft in a single package.

Attitude sensor calibration is required to meet attitude accuracy requirements of modern spacecraft missions. In-space calibration is usually carried out before nominal mission mode operations to compensate for errors induced by launch shock vibration and post-launch disturbances. Numerous factors signify the importance of attitude-independent calibration approaches. For instance, oftentimes the only attitude sensor available during orbit injection is a TAM. Attitude-independent calibration schemes for TAMs have been presented in various papers.[6–10] Most spacecraft missions carry strapped-down gyros as angular rate sensors. Angular rate information is needed in most attitude determination methods, especially for attitude propagation in multi-frame or sequential algorithms. Thus, precise gyro calibration is often the most important of all spacecraft calibrations. Oftentimes, specific maneuvering is planned before a nominal mission to increase the observability of the gyro calibration parameters. Most of the gyro calibration schemes involve estimation of attitude at the same time due to the coupling with attitude in the observation model used.

*Graduate Student, Department of Mechanical & Aerospace Engineering, klai2@ eng.buffalo.edu, Student Member AIAA.

†Associate Professor, Department of Mechanical & Aerospace Engineering, johnc@ eng.buffalo.edu, Associate Fellow AIAA.

‡Aerospace Engineer, Flight Dynamics Analysis Branch, richard.r.harman@ nasa.gov.

In this paper we investigate the possibility of sequential gyro calibration using only TAM measurements, which include the body measurements and inertial reference vectors. In order to incorporate rate information into the effective observation model, a finite difference of the TAM observation is taken. We take advantage of the "clean" nature of the TAM observations, thus noise amplification from taking the derivative of the observation is not of great concern. In fact, the measurement accuracy of modern TAMs exceeds the ephemeris magnetic field model (see Ref. 11 for more details on the nonlinear and non-Gaussian nature of these errors). At this stage, only gyro biases are estimated, but other errors sources such as scale factor errors and/or misalignments can be included as well.

The organization of this paper is as follows: First, the attitude-independent observation model that incorporates the rate information is derived. Then, the Unscented filter is briefly summarized. Next, simulation results are shown, and finally conclusions are drawn.

II. Measurement Model

In this section an attitude-independent TAM measurement model is derived. We first show the gyro model through the common rate-integrating model given by[12]

$$\tilde{\boldsymbol{\omega}}(t) = \boldsymbol{\omega}(t) + \boldsymbol{\beta}(t) + \boldsymbol{\eta}_v(t) \tag{1a}$$

$$\dot{\boldsymbol{\beta}}(t) = \boldsymbol{\eta}_u(t) \tag{1b}$$

where $\tilde{\boldsymbol{\omega}}(t)$ is the continuous-time measured angular rate, $\boldsymbol{\beta}$ is the gyro bias vector in body coordinate, and $\boldsymbol{\eta}_v(t)$ and $\boldsymbol{\eta}_u(t)$ are independent zero-mean Gaussian white-noise processes with

$$E\left\{\boldsymbol{\eta}_v(t)\boldsymbol{\eta}_v^T(\tau)\right\} = I_{3\times3}\sigma_v^2\delta(t-\tau) \tag{2a}$$

$$E\left\{\boldsymbol{\eta}_u(t)\boldsymbol{\eta}_u^T(\tau)\right\} = I_{3\times3}\sigma_u^2\delta(t-\tau) \tag{2b}$$

where $\delta(t-\tau)$ is the Dirac delta function and E denotes expectation. The discrete-time gyro model is given by[13]

$$\tilde{\boldsymbol{\omega}}_{k+1} = \boldsymbol{\omega}_{k+1} + \frac{1}{2}[\boldsymbol{\beta}_{k+1} + \boldsymbol{\beta}_k] + \left[\frac{\sigma_v^2}{\Delta t} + \frac{1}{12}\sigma_u^2\Delta t\right]^{1/2}\mathbf{N}_v \tag{3a}$$

$$\boldsymbol{\beta}_{k+1} = \boldsymbol{\beta}_k + \sigma_u\Delta t^{1/2}\mathbf{N}_u \tag{3b}$$

where $\mathbf{N}_v$ and $\mathbf{N}_u$ are 3×1 zero-mean and independent Gaussian-random vectors with covariances each given by the identity matrix. Also, the subscript k denotes the measurement time index at time $t = t_k$. The discrete-time estimated angular rate is simply

$$\hat{\boldsymbol{\omega}}_k = \tilde{\boldsymbol{\omega}}_k - \hat{\boldsymbol{\beta}}_k \tag{4}$$

A carat will always be used to denote an estimated value, while a tilde will be used to denote a measured value.

Here we assume that the magnetometer has been calibrated for scale factors, non-orthogonality corrections, and biases using one of the attitude independent calibration algorithms, for example, the one presented in Ref. 10. The body frame observation model of a TAM is similar to a typical vector sensor:

$$\tilde{\mathbf{B}}_k = A_k\mathbf{H}_k + \mathbf{v}_k \quad , \quad \mathbf{v}_k \sim \mathcal{N}(\mathbf{0}, \sigma_k^2 I_{3\times3}) \tag{5}$$

where $\tilde{\mathbf{B}}_k$ is the TAM observation, $\mathbf{H}_k$ is the reference magnetic field in an Earth-fixed inertial frame corresponding to the specific orbit and altitude, A_k is the unknown attitude matrix, $\mathbf{v}_k$ is the measurement noise that includes both sensor errors and geomagnetic field model uncertainties, and $I_{3\times3}$ is a 3×3 identity matrix. The measurement noise is assumed to be a zero-mean Gaussian process with covariance $\sigma_k^2 I_{3\times3}$.

Taking a first-order finite difference of the observation model above and using Eq. (5) at times k and $k+1$ yields

$$\begin{aligned}\frac{\tilde{\mathbf{B}}_{k+1} - \tilde{\mathbf{B}}_k}{\Delta t} &= -[\boldsymbol{\omega}_k\times]A_k\mathbf{H}_k + A_k\frac{\mathbf{H}_{k+1} - \mathbf{H}_k}{\Delta t} + \frac{\mathbf{v}_{k+1} - \mathbf{v}_k}{\Delta t} \\ &= -[\boldsymbol{\omega}_k\times]\tilde{\mathbf{B}}_k + [\boldsymbol{\omega}_k\times]\mathbf{v}_k + A_k\frac{\mathbf{H}_{k+1} - \mathbf{H}_k}{\Delta t} + \frac{\mathbf{v}_{k+1} - \mathbf{v}_k}{\Delta t}\end{aligned} \tag{6}$$

where the approximation $(A_{k+1} - A_k)/\Delta t = -[\boldsymbol{\omega}_k\times]A_k$ has been used. This approximation is valid when the spacecraft is rotating slowly compared to the sampling rate, which is true for most on-orbit applications. Also, $[\boldsymbol{\omega}_k\times]$ is the cross product matrix, defined by

$$[\boldsymbol{\omega}_k\times] \equiv \begin{bmatrix} 0 & -\omega_3 & \omega_2 \\ \omega_3 & 0 & -\omega_1 \\ -\omega_2 & \omega_1 & 0 \end{bmatrix} \tag{7}$$

Rearranging Eq. (6) gives

$$A\frac{\mathbf{H}_{k+1} - \mathbf{H}_k}{\Delta t} = \frac{\tilde{\mathbf{B}}_{k+1} - \tilde{\mathbf{B}}_k}{\Delta t} + [\boldsymbol{\omega}_k\times]\tilde{\mathbf{B}}_k - [\boldsymbol{\omega}_k\times]\mathbf{v}_k - \frac{\mathbf{v}_{k+1} - \mathbf{v}_k}{\Delta t} \tag{8}$$

An attitude-independent observation can be derived by computing the norm-square of both sides of Eq. (8):

$$\begin{aligned} \left|\left|\frac{\mathbf{H}_{k+1} - \mathbf{H}_k}{\Delta t}\right|\right|^2 \;=\; & \left|\left|\frac{\tilde{\mathbf{B}}_{k+1} - \tilde{\mathbf{B}}_k}{\Delta t}\right|\right|^2 + \left|\left|[\boldsymbol{\omega}_k\times]\tilde{\mathbf{B}}_k\right|\right|^2 + ||[\boldsymbol{\omega}_k\times]\mathbf{v}_k||^2 + \left|\left|\frac{\mathbf{v}_{k+1} - \mathbf{v}_k}{\Delta t}\right|\right|^2 \\ & +2\left(\frac{\tilde{\mathbf{B}}_{k+1} - \tilde{\mathbf{B}}_k}{\Delta t}\right)\cdot\left([\boldsymbol{\omega}_k\times]\tilde{\mathbf{B}}_k\right) - 2\left(\frac{\tilde{\mathbf{B}}_{k+1} - \tilde{\mathbf{B}}_k}{\Delta t}\right)\cdot([\boldsymbol{\omega}_k\times]\mathbf{v}_k) \\ & -2\left(\frac{\tilde{\mathbf{B}}_{k+1} - \tilde{\mathbf{B}}_k}{\Delta t}\right)\cdot\left(\frac{\mathbf{v}_{k+1} - \mathbf{v}_k}{\Delta t}\right) - 2([\boldsymbol{\omega}_k\times]\tilde{\mathbf{B}}_k)\cdot([\boldsymbol{\omega}_k\times]\mathbf{v}_k) \\ & -2\left([\boldsymbol{\omega}_k\times]\tilde{\mathbf{B}}_k\right)\cdot\left(\frac{\mathbf{v}_{k+1} - \mathbf{v}_k}{\Delta t}\right) + 2([\boldsymbol{\omega}_k\times]\mathbf{v}_k)\cdot\left(\frac{\mathbf{v}_{k+1} - \mathbf{v}_k}{\Delta t}\right) \end{aligned} \tag{9}$$

where $\left|\left|A_k\frac{\mathbf{H}_{k+1}-\mathbf{H}_k}{\Delta t}\right|\right|^2 = \left|\left|\frac{\mathbf{H}_{k+1}-\mathbf{H}_k}{\Delta t}\right|\right|^2$ has been used. The finite-differenced noise can be viewed as

$$\boldsymbol{\varepsilon}_k = \frac{\mathbf{v}_{k+1} - \mathbf{v}_k}{\Delta t} \quad , \quad \boldsymbol{\varepsilon}_k \sim \mathcal{N}(\mathbf{0}, \tilde{\sigma}_k^2 I_{3\times 3}) \quad \text{where} \quad \tilde{\sigma}_k^2 = \frac{2\sigma_k^2}{\Delta t^2} \tag{10}$$

The effective measurement, $\tilde{z}_k$, and effective noise, ν_k, are defined as

$$\tilde{z}_k \equiv \left|\left|\frac{\tilde{\mathbf{B}}_{k+1} - \tilde{\mathbf{B}}_k}{\Delta t}\right|\right|^2 - \left|\left|\frac{\mathbf{H}_{k+1} - \mathbf{H}_k}{\Delta t}\right|\right|^2 \tag{11a}$$

$$\begin{aligned} \nu_k \equiv & -||[\boldsymbol{\omega}_k\times]\mathbf{v}_k||^2 - ||\boldsymbol{\varepsilon}_k||^2 + 2\left(\frac{\tilde{\mathbf{B}}_{k+1} - \tilde{\mathbf{B}}_k}{\Delta t} + [\boldsymbol{\omega}_k\times]\tilde{\mathbf{B}}_k\right)\cdot([\boldsymbol{\omega}_k\times]\mathbf{v}_k) \\ & +2\left(\frac{\tilde{\mathbf{B}}_{k+1} - \tilde{\mathbf{B}}_k}{\Delta t} + [\boldsymbol{\omega}_k\times]\tilde{\mathbf{B}}_k - [\boldsymbol{\omega}_k\times]\mathbf{v}_k\right)\cdot\boldsymbol{\varepsilon}_k \end{aligned} \tag{11b}$$

Thus, after some rearranging Eq. (9) becomes

$$\tilde{z}_k = -\left|\left|[\boldsymbol{\omega}_k\times]\tilde{\mathbf{B}}_k\right|\right|^2 - 2\left(\frac{\tilde{\mathbf{B}}_{k+1} - \tilde{\mathbf{B}}_k}{\Delta t}\right)\cdot\left([\boldsymbol{\omega}_k\times]\tilde{\mathbf{B}}_k\right) + \nu_k \tag{12}$$

The estimate is simply given by

$$\hat{z}_k = -||[\hat{\boldsymbol{\omega}}_k\times]\tilde{\mathbf{B}}_k||^2 - 2\left(\frac{\tilde{\mathbf{B}}_{k+1} - \tilde{\mathbf{B}}_k}{\Delta t}\right)\cdot\left([\hat{\boldsymbol{\omega}}_k\times]\tilde{\mathbf{B}}_k\right) \tag{13}$$

where $\hat{\boldsymbol{\omega}}_k$ is given by Eq. (4).

The mean and variance of the effective measurement noise, ν_k, are now computed. The mean of ν_k is given by

$$\bar{\mu}_k \equiv E\{\nu_k\} = -2\sigma_k^2\boldsymbol{\omega}_k^T\boldsymbol{\omega}_k - \mathrm{Tr}(\tilde{\sigma}_k^2 I_{3\times 3}) = -2\sigma_k^2\boldsymbol{\omega}_k^T\boldsymbol{\omega}_k - \frac{6\sigma_k^2}{\Delta t^2} \approx -\frac{6\sigma_k^2}{\Delta t^2} \tag{14}$$

We now show the validity of the approximation in Eq. (14). If the bandwidth of the attitude variations (i.e., the frequency content) is well below the Nyquist frequency, with a safety factor of 10, then $||\boldsymbol{\omega}_k||\,\Delta t < \pi/10$ for all k. This condition obviously holds when the spacecraft is rotating slowly compared to the sampling rate, which is required by the assumptions made leading to Eq. (6). Then, the following inequality is true:

$$2\sigma_k^2 \boldsymbol{\omega}_k^T \boldsymbol{\omega}_k < \frac{2\pi^2\sigma_k^2}{100\,\Delta t^2} << \frac{6\sigma_k^2}{\Delta t^2} \tag{15}$$

Thus, the approximation in Eq. (14) is valid to within an order of magnitude. The expectation of the square of ν_k is now determined. We write down only those "interesting" terms (excluding those terms that are clearly zero):

$$\begin{aligned} E\{\nu_k^2\} &= E\left\{ \overset{①}{\left(\|[\boldsymbol{\omega}_k\times]\mathbf{v}_k\|^2\right)^2} \right\} + 2E\left\{ \overset{②}{\|[\boldsymbol{\omega}_k\times]\mathbf{v}_k\|^2 \|\boldsymbol{\varepsilon}_k\|^2} \right\} + E\left\{ \overset{③}{\left(\|\boldsymbol{\varepsilon}_k\|^2\right)^2} \right\} \\ &\quad +4E\left\{ \overset{④}{\left[\left(\frac{\tilde{\mathbf{B}}_{k+1}-\tilde{\mathbf{B}}_k}{\Delta t} + [\boldsymbol{\omega}_k\times]\tilde{\mathbf{B}}_k \right) \cdot ([\boldsymbol{\omega}_k\times]\mathbf{v}_k) \right]^2} \right\} \\ &\quad +4E\left\{ \overset{⑤}{\left[\left(\frac{\tilde{\mathbf{B}}_{k+1}-\tilde{\mathbf{B}}_k}{\Delta t} + [\boldsymbol{\omega}_k\times]\tilde{\mathbf{B}}_k \right) \cdot \boldsymbol{\varepsilon}_k \right]^2} \right\} + 4E\left\{ \overset{⑥}{\left[([\boldsymbol{\omega}_k\times]\mathbf{v}_k) \cdot \boldsymbol{\varepsilon}_k \right]^2} \right\} \end{aligned} \tag{16}$$

This equation can be simplified by applying a Monte-Carlo style simulation to investigate what terms in Eq. (16) have the most dominant effects. Table 1 shows the parameters used for two cases: one from a typical low-Earth point spacecraft mission (Case 1) and the other one that is spinning 10 times faster (Case 2). The means and 3σ bounds of the terms in Eq. (16) are computed for these two cases. From Table 2 we can see that for both cases the most dominate terms are given by ③, ④ and ⑤. Thus, the remaining terms can essentially be ignored. Carrying out the expectation of ③, ④ and ⑤, the approximated variance now becomes

$$\begin{aligned} \bar{\sigma}_k^2 &\equiv \mathrm{E}\{\nu_k^2\} - \bar{\mu}_k^2 \\ &= 4\left(\frac{\tilde{\mathbf{B}}_{k+1}-\tilde{\mathbf{B}}_k}{\Delta t} + [\boldsymbol{\omega}_k\times]\tilde{\mathbf{B}}_k \right)^T [\boldsymbol{\omega}_k\times]^T \sigma_k^2 I_{3\times3} [\boldsymbol{\omega}_k\times] \left(\frac{\tilde{\mathbf{B}}_{k+1}-\tilde{\mathbf{B}}_k}{\Delta t} + [\boldsymbol{\omega}_k\times]\tilde{\mathbf{B}}_k \right) \\ &\quad +4\left(\frac{\tilde{\mathbf{B}}_{k+1}-\tilde{\mathbf{B}}_k}{\Delta t} + [\boldsymbol{\omega}_k\times]\tilde{\mathbf{B}}_k \right)^T \tilde{\sigma}_k^2 I_{3\times3} \left(\frac{\tilde{\mathbf{B}}_{k+1}-\tilde{\mathbf{B}}_k}{\Delta t} + [\boldsymbol{\omega}_k\times]\tilde{\mathbf{B}}_k \right) + 2\left[\mathrm{Tr}(\tilde{\sigma}_k^2 I_{3\times3})\right]^2 \\ &= -4\sigma_k^2 \left(\frac{\tilde{\mathbf{B}}_{k+1}-\tilde{\mathbf{B}}_k}{\Delta t} + [\boldsymbol{\omega}_k\times]\tilde{\mathbf{B}}_k \right)^T [\boldsymbol{\omega}_k\times]^2 \left(\frac{\tilde{\mathbf{B}}_{k+1}-\tilde{\mathbf{B}}_k}{\Delta t} + [\boldsymbol{\omega}_k\times]\tilde{\mathbf{B}}_k \right) \\ &\quad +\frac{8\sigma_k^2}{\Delta t^2} \left(\frac{\tilde{\mathbf{B}}_{k+1}-\tilde{\mathbf{B}}_k}{\Delta t} + [\boldsymbol{\omega}_k\times]\tilde{\mathbf{B}}_k \right)^T \left(\frac{\tilde{\mathbf{B}}_{k+1}-\tilde{\mathbf{B}}_k}{\Delta t} + [\boldsymbol{\omega}_k\times]\tilde{\mathbf{B}}_k \right) + \frac{72\sigma_k^4}{\Delta t^4} \end{aligned} \tag{17}$$

Since the measurement noise is small compared to the geomagnetic field,[14] then to a large degree, ν_k can be approximated to be

$$\nu_k \sim \mathcal{N}(\bar{\mu}_k, \bar{\sigma}_k^2) \tag{18}$$

Note that in Eq. (17) the measurement, $\tilde{\mathbf{B}}_k$, is actually a random variable equal to $\mathbf{B}_k^{\mathrm{true}} + \mathbf{v}_k$. However, the error introduced by using the measurement instead of the true value is very small, since $\bar{\mu}_k^2 \ll \bar{\sigma}_k^2$, by nearly four orders of magnitude if we do not exceed 70 deg in magnetic latitude.[14] Also, the true angular velocity is not known, but by the same analogy a measured (or in our case an estimated) angular velocity can be used in the variance.

Table 1. Parameters Used for the Different Cases

	Case 1	Case 2
σ_k (mG)	0.5	0.5
Δt (s)	10	10
$\boldsymbol{\omega}_k$ (rad/s)	0.00114416 (or 236 deg/hr, 3-axis)	0.0114416 (or 2360 deg/hr, 3-axis)
$\tilde{\mathbf{B}}_k$ (mG)	$[-63.8352\ 224.2383\ 20.9083]^T$	$[-63.8352\ 224.2383\ 20.9083]^T$
$\tilde{\mathbf{B}}_{k+1}$ (mG)	$[-63.6305\ 225.4403\ 22.6389]^T$	$[-56.7669\ 232.4573\ 42.1828]^T$

Table 2. Mean and 3σ Bounds of the Terms

	Case 1	Case 2
①	$(7.6940 \pm 0.2377) \times 10^{-12}$	$(7.7060 \pm 0.1167) \times 10^{-8}$
②	$(7.8379 \pm 0.2189) \times 10^{-8}$	$(7.8439 \pm 0.1255) \times 10^{-6}$
③	$(3.7453 \pm 0.0847) \times 10^{-4}$	$(3.7506 \pm 0.0795) \times 10^{-4}$
④	$(1.0429 \pm 0.0099) \times 10^{-6}$	$(1.0832 \pm 0.0159) \times 10^{-2}$
⑤	$(5.9596 \pm 0.1161) \times 10^{-3}$	$(6.4093 \pm 0.0931) \times 10^{-1}$
⑥	$(1.9648 \pm 0.0513) \times 10^{-8}$	$(1.9532 \pm 0.0404) \times 10^{-6}$
Total	$(6.3354 \pm 0.1264) \times 10^{-3}$	$(6.5204 \pm 0.1042) \times 10^{-1}$

III. Unscented Filter Formulation

In this section a new approach, developed by Julier, Uhlmann and Durrant-Whyte,[15] is discussed as an alternative to the EKF. This approach, which they called the *Unscented filter* (UF), works on the premise that with a fixed number of parameters it should be easier to approximate a Gaussian distribution than to approximate an arbitrary nonlinear function. The Unscented filter uses a different propagation than the form given by the standard extended Kalman filter. Given an $n \times n$ covariance matrix P, a set of order n points can be generated from the columns (or rows) of the matrices $\pm\sqrt{nP}$. The set of points is zero-mean, but if the distribution has mean $\boldsymbol{\mu}$, then simply adding $\boldsymbol{\mu}$ to each of the points yields a symmetric set of $2n$ points having the desired mean and covariance. Due to the symmetric nature of this set, its odd central moments are zero, so its first three moments are the same as the original Gaussian distribution (see Ref. 16 for more details).

The filter presented in Ref. 15 is derived for discrete-time nonlinear equations, where the system model is given by

$$\mathbf{x}_{k+1} = \mathbf{f}(\mathbf{x}_k,\, k) + G_k \mathbf{w}_k \tag{19a}$$

$$\tilde{\mathbf{y}}_k = \mathbf{h}(\mathbf{x}_k,\, k) + \mathbf{v}_k \tag{19b}$$

The vectors $\mathbf{w}_k$ and $\mathbf{v}_k$ are zero-mean Gaussian noise processes with covariances given by Q_k and R_k,

respectively. The implementation of the UF for real-time gyro-bias calibration using magnetometer data is straightforward. Only the relevant equations used for the gyro-bias calibration problem are shown here. First, the following set of *sigma points* are computed from $P_k + \bar{Q}$:

$$\boldsymbol{\sigma}_k \leftarrow 2n \text{ columns from } \pm\gamma\sqrt{P_k + \bar{Q}_k} \tag{20a}$$

$$\boldsymbol{\chi}_k(0) = \hat{\mathbf{x}}_k \tag{20b}$$

$$\boldsymbol{\chi}_k(i) = \boldsymbol{\sigma}_k(i) + \hat{\mathbf{x}}_k, \quad i = 1,\, 2,\, \ldots,\, 2n \tag{20c}$$

The relationship of the quantity $\bar{Q}_k$ to Q_k will be discussed shortly. The parameter γ is given by $\gamma = \sqrt{n + \lambda}$, where the composite scaling parameter, λ, is given by $\lambda = \alpha^2(n + \kappa) - n$. The constant α determines the spread of the sigma points and is usually set to a small positive value (e.g. $1 \times 10^{-4} \leq \alpha \leq 1$).[16] Also, the parameter κ is usually given by $\kappa = 3 - n$. Efficient methods to compute the matrix square root can be found by using the Cholesky decomposition.[17] The following weights are now defined:

$$W_0^{\text{mean}} = \frac{\lambda}{n + \lambda} \tag{21a}$$

$$W_0^{\text{cov}} = \frac{\lambda}{n + \lambda} + (1 - \alpha^2 + \beta) \tag{21b}$$

$$W_i^{\text{mean}} = W_i^{\text{cov}} = \frac{1}{2(n + \lambda)}, \quad i = 1,\, 2,\, \ldots,\, 2n \tag{21c}$$

where β is used to incorporate prior knowledge of the distribution (for Gaussian distributions $\beta = 2$ is optimal).

The state vector, $\mathbf{x}$, consists of the gyro biases $\boldsymbol{\beta}$. Since the state model estimate is given by $\dot{\hat{\mathbf{x}}}(t) = \mathbf{0}$, then the propagated values for the state and covariance are given by their respective updated values, which significantly reduces the computational requirements in the UF. Hence, the only essential difference between the EKF and UF formulations is in the computation of the innovations covariance, where the EKF uses a first-order expansion to compute this quantity, while the UF uses a nonlinear transformation to compute this quantity. For the gyro-bias calibration algorithm using the UF, the state estimate is calculated by

$$\hat{\mathbf{x}}_{k+1} = \hat{\mathbf{x}}_k + K_k(\tilde{z}_{k+1} - \hat{y}_k) \tag{22}$$

where $\hat{y}_k$ is the mean observation, given by

$$\hat{y}_k = \sum_{i=0}^{2n} W_i^{\text{mean}}\, h\left[\boldsymbol{\chi}_k(i)\right] \tag{23}$$

The quantity $h\left[\boldsymbol{\chi}_k(i)\right]$ is defined by

$$h\left[\boldsymbol{\chi}_k(i)\right] = -||[\hat{\boldsymbol{\omega}}_k\times]\tilde{\mathbf{B}}_k||^2 - 2\left(\frac{\tilde{\mathbf{B}}_{k+1} - \tilde{\mathbf{B}}_k}{\Delta t}\right) \cdot \left([\hat{\boldsymbol{\omega}}_k\times]\tilde{\mathbf{B}}_k\right) \tag{24}$$

where $\hat{\boldsymbol{\omega}}_k = \tilde{\boldsymbol{\omega}}_k - \boldsymbol{\chi}_k(i)$ is used in Eq. (24). The gain K_k is computed by

$$K_k = P_k^{xy}[P_k^{yy} + \bar{\sigma}_k^2(\hat{\mathbf{x}}_k)]^{-1} \tag{25}$$

where $\bar{\sigma}_k^2(\hat{\mathbf{x}}_k)$ is given by Eq. (17). This variable is a function of the estimated state, which means that the estimated angular velocity is used to compute this variance. Also, P_k^{xy} is the cross-correlation matrix between $\hat{\mathbf{x}}_k$ and $\hat{y}_k$, given by

$$P_k^{xy} = \sum_{i=0}^{2n} W_i^{\text{cov}}\, \left\{\boldsymbol{\chi}_k^x(i) - \hat{\mathbf{x}}_k\right\}\, \left\{h\left[\boldsymbol{\chi}_k(i)\right] - \hat{y}_k\right\}^T \tag{26}$$

and P_k^{yy} is the output covariance, given by

$$P_k^{yy} = \sum_{i=0}^{2n} W_i^{\text{cov}}\, \left\{h\left[\boldsymbol{\chi}_k(i)\right] - \hat{y}_k\right\}\, \left\{h\left[\boldsymbol{\chi}_k(i)\right] - \hat{y}_k\right\}^T \tag{27}$$

Finally, the propagated covariance is given by

$$P_{k+1} = P_k - K_k[P_k^{yy} + \bar{\sigma}_k^2(\hat{\mathbf{x}}_k)]K_k^T + \bar{Q}_k \tag{28}$$

New sigma points can now be calculated using P_{k+1} for the sequential UF process.

We now discuss the variable $\bar{Q}_k$. Various methods can be used to handle the process noise and measurement noise in the UF. Reference [16] states that if the process noise is purely additive in the model, then its covariance can simply be added using a simple additive procedure. Reference [18] expand upon this concept by incoporating an approximation for the integration over the sampling interval, which more closely follows the actual process. Any process noise that is added to the state vector in the UF is effectively multiplied by the state transition matrix, $\Phi(\Delta t)$, which gives $\Phi(\Delta t)Q_k\Phi^T(\Delta t)$ at the end of the interval. This mapping is done automatically by the state propagation, and does not need to be explicitly accounted for in the propagation. However, adding equal process noise at the beginning and end of the propagation might yield better results. The total desired process noise follows

$$\Phi(\Delta t)\bar{Q}_k\Phi^T(\Delta t) + \bar{Q}_k = G_kQ_kG_k^T \tag{29}$$

where $\bar{Q}_k$ is used in Eq. (20a) and in the calculation of the predicted covariance in Eq. (28). This approach is similar to a trapezoid rule for integration. In this paper, both $\Phi(\Delta t)$ and G_k are identity matrices, thus we obtain the simple relationship $\bar{Q}_k = Q_k/2 = (\sigma_u^2\Delta t/2)I_{3\times 3}$. Also, note that the filter does not use σ_v^2 anywhere. This is due to the fact that $\tilde{\boldsymbol{\omega}}_k$ is not used to drive a kinematics model, commonly found in the standard attitude estimation problem.[19] In theory, Eq. (3a) should be substituted into Eq. (12) to compute the variance of the effective measurement, which will now involve σ_v^2. But, as stated previously, the errors introduced by using the estimated angular velocity are negligible.

IV. Simulation Results

In this section we show simulation results of the new formulation to estimate the gyro biases from magnetometer measurements. The simulated spacecraft is modelled after the Tropical Rainfall Measurement Mission (TRMM), which was successfully launched on November 27, 1997. The mission is to study the properties of tropical and subtropical rainfall including the effect of El Niño on rainfall. Currently, this Earth-pointing spacecraft is at a near-circular orbit of 402 km with an inclination of 35°. In this formulation, we needed only the rate information from the gyros, the TAM observations and its corresponding Earth-fixed reference values. The magnetic field is simulated using a 10^{th}-order International Geomagnetic Reference Field model.[11] The magnetometer-body and geomagnetic-reference vectors for the simulated runs each have a magnitude of about 500 mG. The measurements are sampled every 10 seconds over an 8 hour span.

The parameters for UF are chosen to be

$$\alpha = 1, \qquad \beta = 2, \qquad \kappa = 3 - n = 0 \tag{30}$$

where $n = 3$. The standard deviations of the gyro noise and gyro bias random walk noise are given by

$$\sigma_v = 0.31623 \ \mu\text{rad/sec}^{1/2}, \qquad \sigma_u = 3.1623 \times 10^{-4}\mu\text{rad/sec}^{3/2} \tag{31}$$

and the TAM measurement noise given by

$$\sigma_k = 0.5 \text{ mG} \tag{32}$$

The initial gyro biases are given by

$$\boldsymbol{\beta}_0 = \begin{bmatrix}\beta_x(t_0)\\ \beta_y(t_0)\\ \beta_z(t_0)\end{bmatrix} = \begin{bmatrix}10\\ -30\\ 20\end{bmatrix} \text{ deg/hr} \tag{33}$$

These values are used in order to test the performance of the UF to estimate the biases from large initial errors. The UF is executed at time $t = 0$ with no a priori knowledge of the gyro-bias parameters (i.e., $\hat{\mathbf{x}}_0 = \mathbf{0}$). The initial error covariance for the gyro biases estimate is chosen to be $P_0 = 10^2 I_{3\times 3}$ deg^2/hr^2, which bounds the initial bias errors in a 3σ sense.

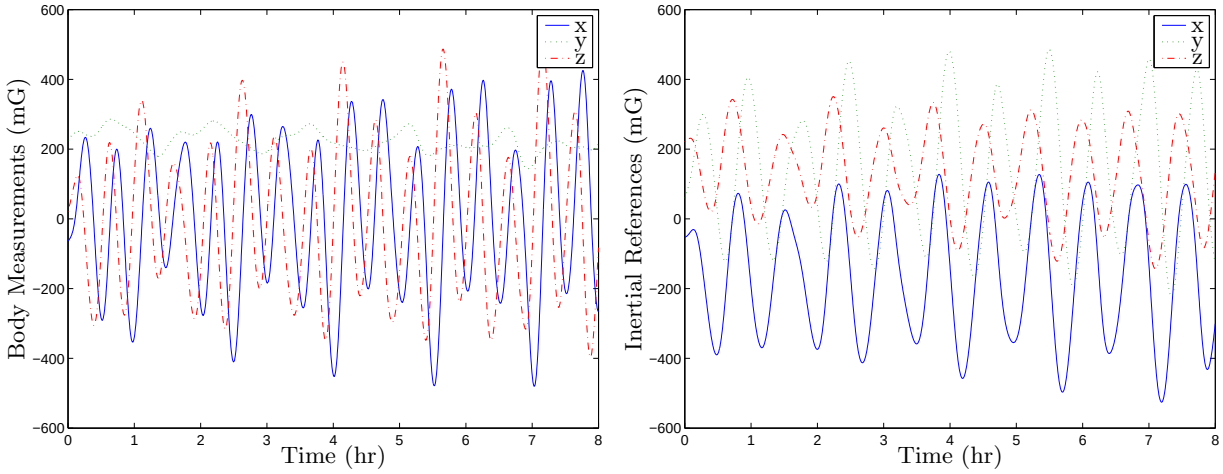

(a) Measured (b) Inertial Reference

Figure 1. Magnetic Field

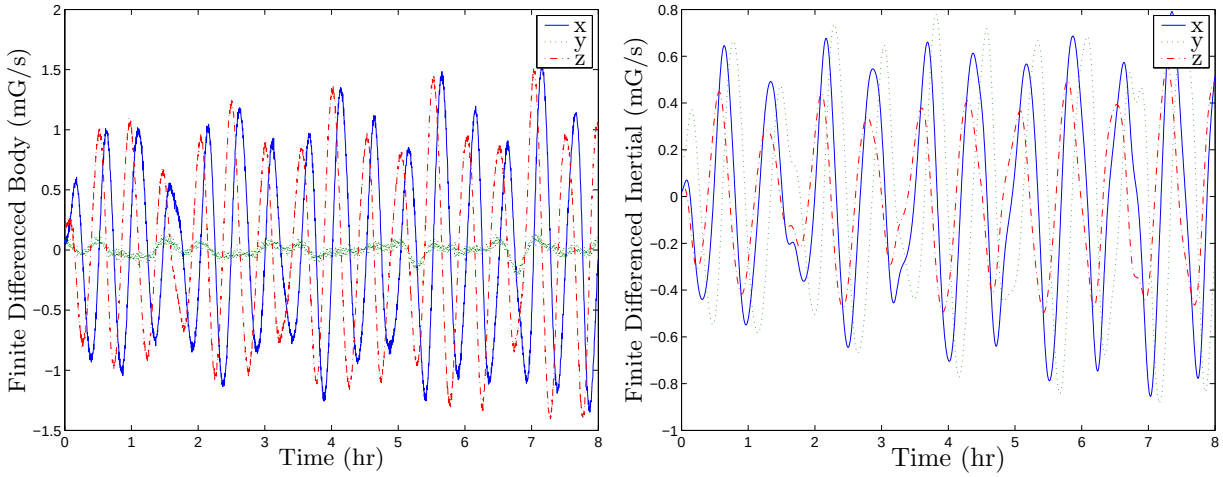

(a) Measured (b) Inertial Reference

Figure 2. Magnetic Field Rate

Figure 1 shows the TAM measurements and the corresponding reference magnetic field, and Figure 2 shows their rates obtained from the finite difference. Also, the effective measurement is plotted in Figure 3, which indicates good motion. (In general, more motion in the measurements produces a more "observable" scenario for the to-be-estimated biases.) Figure 4 shows the angular velocity outputs before and after calibration. Note that the gyro measurement does not significantly "drift" in this time span, which is due to the high quality gyro used in the simulation. We can see that the new calibration approach successfully estimated the gyro biases. The calibration errors with their corresponding 3σ bounds of the gyro biases are shown in Figure 5. This is another way of showing the effectiveness of the new algorithm. Good convergence properties leading to accurate bias estimates are given. Since the spacecraft is spinning about its y-axis, the y-axis gyro bias has slightly lower error covariance than the other axes.

The robustness of the UF algorithm is also tested by adding colored noise to the measurements, which more closely models the actual geomagnetic field errors. This noise is modelled using the colored noise model shown in Ref. 20. The results obtained are nearly identical to the results shown in Figure 5, unlike the results for the magnetometer calibration algorithms of Ref. 10. Therefore, the gyro-bias determination algorithm is

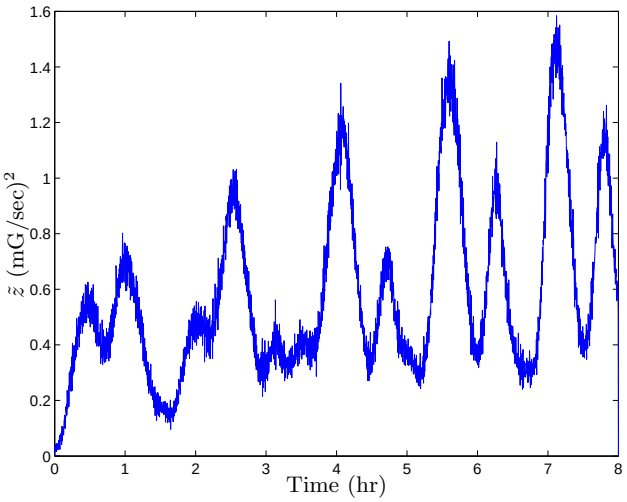

Figure 3. Effective Measurement

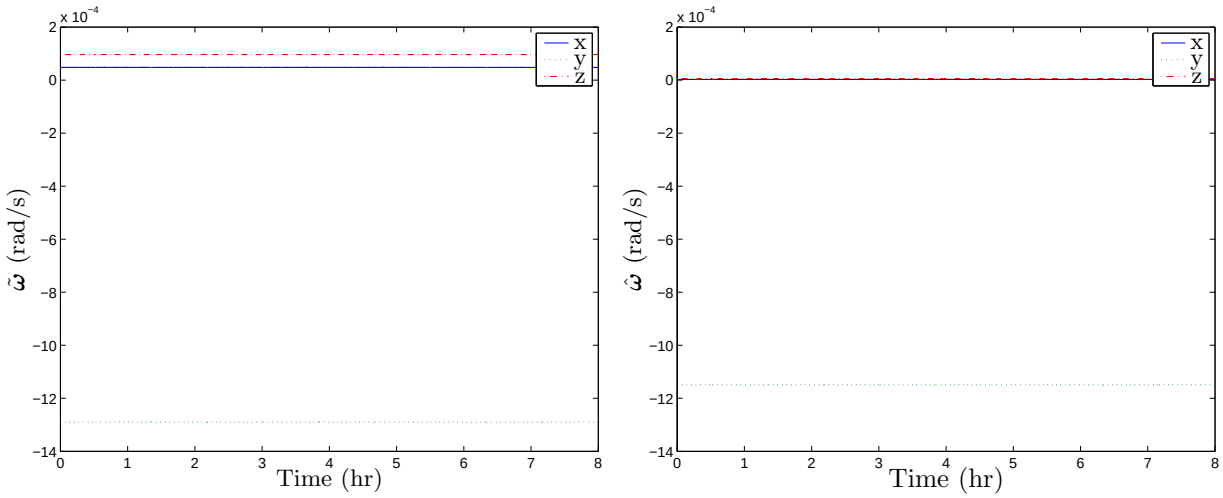

(a) Pre-calibrated (b) Calibrated

Figure 4. Angular Velocity Outputs

robust to realistic errors in the geomagnetic field.

V. Conclusions

In this paper a new formulation for gyro-bias calibration was derived that works on the velocity level of the magnetometer measurements and the reference magnetic field. The UF was the preferred filter over the EKF for the robustness properties especially to large initial errors. Simulation results indicate that the new approach can successfully estimate for the gyro biases using magnetometer measurements without attitude knowledge. These encouraging results pave the way for a more advanced formulation involving full calibration of the gyro biases as well as scale factors and non-orthogonality corrections.

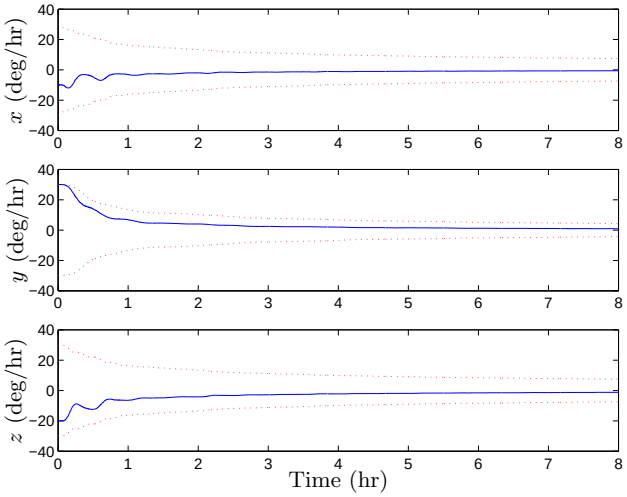

Figure 5. Gyro Bias Estimation Errors with 3σ Bounds

Acknowledgments

The first author would like to thank Dr. Yang Cheng of University at Buffalo for his assistance and constructive discussions. The authors also would like to express gratitude to Dr. F. Landis Markley of NASA-Goddard Space Flight Center for his notes that lead to the derivation of statistically correct gyro noise model. This research was supported by NASA-Goddard Space Flight Center grant NAG5-12179. The first author's graduate studies are supported by this grant. This author greatly appreciates the support.

References

[1]Blaylock, B. T., "Magnetometers," *Spacecraft Attitude Determination and Control*, edited by J. R. Wertz, chap. 6.3, Kluwer Academic Publishers, The Netherlands, 1978, pp. 180–184.

[2]Psiaki, M. L., Martel, F., and Pal, P. K., "Three-Axis Attitude Determination via Kalman Filtering of Magnetometer Data," *Journal of Guidance, Control, and Dynamics*, Vol. 13, No. 3, May-June 1990, pp. 506–514.

[3]Challa, M. and Natanson, G., "Effects of Magnetometer Calibration and Maneuvers on Accuracies of Magnetometer-Only Attitude and Rate Determination," *Proceedings of the AAS/GSFC 13th International Symposium on Space Flight Dynamics*, Vol. 1, (NASA/CP-1998-206858/VOL1) NASA-Goddard Space Flight Center, Greenbelt, MD, May 1998, pp. 389–401.

[4]Deutschmann, J. K. and Bar-Itzhack, I., "Evaluation of Attitude and Orbit Estimation Using Actual Earth Magnetic Field Data," *Journal of Guidance, Control, and Dynamics*, Vol. 24, No. 3, May-June 2001, pp. 616–623.

[5]Jung, J. and Psiaki, M. L., "Tests of Magnetometer/Sun-Sensor Orbit Determination Using Flight Data," *Journal of Guidance, Control, and Dynamics*, Vol. 25, No. 3, May-June 2002, pp. 582–590.

[6]Alonso, R. and Shuster, M. D., "Complete Linear Attitude-Independent Magnetometer Calibration," *Journal of the Astronautical Sciences*, Vol. 50, No. 4, Oct.-Dec. 2002, pp. 477–490.

[7]Alonso, R. and Shuster, M. D., "Attitude-Independent Magnetometer-Bias Determination: A Survey," *Journal of the Astronautical Sciences*, Vol. 50, No. 4, Oct.-Dec. 2002, pp. 453–475.

[8]Alonso, R. and Shuster, M. D., "Centering and Observability in Attitude-Independent Magnetometer-Bias Determination," *Journal of the Astronautical Sciences*, Vol. 51, No. 2, Apr.-June 2003, pp. 133–141.

[9]Alonso, R. and Shuster, M. D., "A New Algorithm for Attitude-Independent Magnetometer Calibration," *Proceedings of the Flight Mechanics/Estimation Theory Symposium*, (NASA/CP-3265) NASA-Goddard Space Flight Center, Greenbelt, MD, May 1994, pp. 513–527.

[10]Crassidis, J. L., Lai, K.-L., and Harman, R. R., "Real-Time Attitude-Independent Three-Axis Magnetometer Calibration," *Flight Mechanics Symposium*, (NASA CP-2003-212246) NASA-Goddard Space Flight Center, Greenbelt, MD, Oct. 2003, Session 6, Paper 5.

[11]Langel, R. A., "The Main Field," *Geomagnetism*, edited by J. A. Jacobs, Academic Press, Orlando, FL, 1987, pp. 249–512.

[12]Farrenkopf, R. L., "Analytic Steady-State Accuracy Solutions for Two Common Spacecraft Attitude Estimators," *Journal of Guidance, Control, and Dynamics*, Vol. 1, No. 4, July-Aug. 1978, pp. 282–284.

[13]Markley, F. L., *Private Communication*.

[14]Alonso, R. and Shuster, M. D., "TWOSTEP: A Fast Robust Algorithm for Attitute-Independent Magnetometer-Bias Determination," *Journal of the Astronautical Sciences*, Vol. 50, No. 4, Oct.-Dec. 2002, pp. 433–451.

[15]Julier, S. J., Uhlmann, J. K., and Durrant-Whyte, H. F., "A New Method for the Nonlinear Transformation of Means and Covariances in Filters and Estimators," *IEEE Transactions on Automatic Control*, Vol. AC-45, No. 3, March 2000, pp. 477–482.

[16]Wan, E. and van der Merwe, R., "The Unscented Kalman Filter," *Kalman Filtering and Neural Networks*, edited by S. Haykin, chap. 7, Wiley, 2001.

[17]Golub, G. H. and Van Loan, C. F., *Matrix Computations*, The Johns Hopkins University Press, Baltimore, MD, 2nd ed., 1989.

[18]Crassidis, J. L. and Markley, F. L., "Unscented Filtering for Spacecraft Attitude Estimation," *AIAA Guidance, Navigation, and Control Conference*, Austin, TX, Aug. 2003.

[19]Lefferts, E. J., Markley, F. L., and Shuster, M. D., "Kalman Filtering for Spacecraft Attitude Estimation," *Journal of Guidance, Control, and Dynamics*, Vol. 5, No. 5, Sept.-Oct. 1982, pp. 417–429.

[20]Alonso, R. and Shuster, M. D., "TWOSTEP: A Fast Robust Algorithm for Attitude-Independent Magnetometer-Bias Determination," *Journal of the Astronautical Sciences*, Vol. 50, No. 4, Oct.-Dec. 2002, pp. 433–451.